Optica Acta: International Journal of Optics

ISSN: 0030-3909 (Print) (Online) Journal homepage: https://www.tandfonline.com/loi/tmop19

A Mode Selector to Suppress Fluctuations in Laser Beam Geometry

A. Rüdiger , R. Schilling , L. Schnupp , W. Winkler , H. Billing & K. Maischberger

To cite this article: A. Rüdiger , R. Schilling , L. Schnupp , W. Winkler , H. Billing & K. Maischberger (1981) A Mode Selector to Suppress Fluctuations in Laser Beam Geometry, Optica Acta: International Journal of Optics, 28:5, 641-658, DOI: 10.1080/713820609

To link to this article: https://doi.org/10.1080/713820609

Published online: 14 Nov 2010.

OPTICA ACTA, 1981, VOL. 28, NO. 5, 641–658

A mode selector to suppress fluctuations in laser beam geometry

A. RÜDIGER, R. SCHILLING, L. SCHNUPP,
W. WINKLER, H. BILLING and K. MAISCHBERGER

Max-Planck-Institut für Physik und Astrophysik, Institut für Astrophysik, D-8046 Garching bei München, F.R. Germany

(*Received 3 July 1980; revision received 11 July 1980*)

Abstract. Our development of a gravitational wave detector requires a Michelson interferometer of extreme sensitivity capable of measuring 10^{-16} m (i.e. some 10^{-10} of a wavelength λ of the illuminating laser light). Even after painstaking alignment of the interferometer components, and after considerable improvement of the laser stability, noise contributions much in excess of this goal were observed, due partly to fluctuations of the laser beam geometry. The two most obvious types of geometric beam fluctuations are a lateral beam jitter and a pulsation in beam width; these lead to spurious interferometer signals if the interfering wavefronts are misaligned in their tilts or in their curvatures respectively.

The geometry of the laser beam can be considerably stabilized by passing it through an optical resonator. The geometric beam fluctuations, as viewed from this resonator, can be described by a well-centred ground mode TEM_{00}, contaminated by transverse modes TEM_{mn}, with amplitudes decreasing rapidly with the mode order $m+n$. In the simplest case, the resonator consists of two identical concave mirrors of high reflectance ρ^2. The mirror separation can be chosen such that, while the resonator is tuned for maximum transmittance for the TEM_{00} mode, the low order transverse modes TEM_{mn} are almost totally suppressed, in amplitude by factors of the order of $1-\rho^2$. Considerations leading to a practical implementation are discussed, and experimental results are given.

1. Introduction

The gravitational wave detector being developed [1, 2] at the Max-Planck-Institut für Physik und Astrophysik is intended to measure the small strains $\delta L/L$ induced by gravitational radiation. The most promising sources are catastrophic events lasting only a few milliseconds, which transmit their largest spectral contributions in the range from a few hundred to a few thousand hertz. The goal is to reach a sensitivity $\delta L/L$ of about 10^{-21} so as to be able to detect events as far away as the Virgo cluster.

1.1. *A Michelson interferometer*

The detector is a laser-illuminated Michelson interferometer. Its total optical path length L has an optimum at half the wavelength of the gravitational radiation, say 100 km. One can realize such long paths by reflecting the interferometer beam N times (e.g. several hundred times) between two concave mirrors at distance l, as indicated in figure 1 for $N=4$ passes. But even then, variations δL in path difference of as little as 10^{-16} m have to be measured, i.e. some 10^{-10} of a wavelength λ of the

0030-3909/81/2805-0641 $02.00

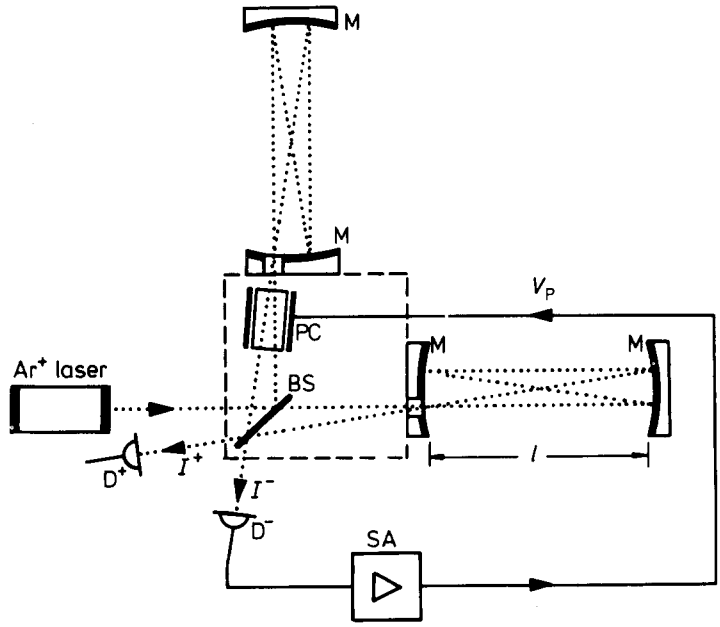

Figure 1. Michelson interferometer with folded light paths $L = Nl$, $N = 4$. BS beam splitter; M mirror; PC Pockels cell; D^+, D^- photodiodes; SA servo amplifier.

illuminating laser light (Ar^+ laser, $\lambda = 514\,\text{nm}$). Throughout this paper, path differences δL will be expressed by the resulting phase differences

$$\phi = k\delta L = 2\pi\delta L/\lambda, \tag{1.1}$$

with $k = 2\pi/\lambda$ the propagation constant. In terms of these phase differences, our sensitivity goal ϕ_g is of the order of 10^{-9} rad. The interference of the recombined beams is monitored at one or both of the output ports by photodiodes D^+ and D^-, where, for parallel wavefronts, the light powers $P^\pm$ would be

$$P^\pm = \frac{P_0}{2}(1 \pm \cos\Phi). \tag{1.2}$$

A chosen operating point Φ_0 is maintained via a servo loop, by applying a voltage $V_P(t)$ to a Pockels cell such that the change in optical phase $\chi(t)$ in the Pockels material compensates the changes in geometric phase $\phi_0(t)$:

$$\Phi_0 = \phi_0(t) - \chi(t) = \text{const.} \tag{1.3}$$

One choice [3] of the operating point is to make the two output powers equal; the other [4], which we have adopted, uses a modulation technique, allowing operation at a power minimum of P^-, i.e. at

$$\Phi_0 = 0 \bmod 2\pi. \tag{1.4}$$

Both choices represent nulling methods, making the measured signal $\chi(t)$ very insensitive to fluctuations in the laser power.

1.2. *Local phase variations and field fluctuations*

This paper is concerned with the noise effects that can arise when—in contrast to the assumptions of equation (1.2)—the interfering wavefronts are not parallel, but rather arrive at the photodiode D^- (x,y-plane) with a phase difference

$$\Phi(x, y; t) = \phi(x, y; t) - \chi(t) \tag{1.5}$$

that is a function of x and y, owing to imperfections in the interferometer. In the presence of such local phase variations $\phi(x, y; t)$, the Pockels signal $\chi(t)$ becomes a function of the (possibly time-dependent) field distributions $E_1(x, y; t)$, $E_2(x, y; t)$ of the two interfering beams.

Quite generally, the light power $P(t)$ striking the photodiode D^- can be written as

$$P(t) = \frac{1}{2Z} \int\int |E_1 - E_2 \exp(i\Phi)|^2 \, dxdy, \tag{1.6}$$

or, showing more clearly the phase dependence,

$$P(t) = \frac{1}{2Z} \int\int \{E_1^2 + E_2^2 - 2E_1 E_2 \cos \Phi\} \, dxdy \tag{1·7}$$

(with $Z = \sqrt{(\varepsilon_0/\mu_0)}$ the vacuum impedance). For sufficiently narrow beams, the integration over the photodiode surface can be replaced by an integration over the infinite plane x,y.

The interferometer signal is given by the Pockels cell phase $\chi(t)$, which is servo-controlled in such a way as to make the power $P(t)$ on the photodiode a minimum. A necessary condition for a minimum is $\partial P/\partial \chi = 0$, which leads to

$$\tan \chi(t) = \frac{\int\int E_1 E_2 \sin \phi \, dxdy}{\int\int E_1 E_2 \cos \phi \, dxdy}, \tag{1.8}$$

where E_1, E_2 and ϕ are functions of x, y and t. If $\chi_{\min}(t)$ is a solution leading to a power minimum, so are the solutions given by $\chi_{\text{even}}(t) = \chi_{\min}(t) \bmod 2\pi$, whereas the odd solutions $\chi_{\text{odd}}(t) = \chi_{\text{even}}(t) + \pi$ would lead to power maxima on the photodiode.

1.3. *The error signal*

We will narrow down the discussion to cases in which the geometric phase can be written

$$\phi(x, y; t) = \phi_0(t) + \bar{\phi}(x, y), \tag{1.9}$$

i.e. separated into a main signal $\phi_0(t)$ and a stationary phase 'ripple' $\bar{\phi}(x, y)$ that does not depend on the time t.

Such time-independent variations $\bar{\phi}(x, y)$ in the geometric phase can result from misalignments of the beam splitter, or from mismatches between the optical components in the two interferometer arms. They can nevertheless lead to time-dependent spurious fluctuations $\delta\chi(t)$ in the compensating signal $\chi(t)$ if the interfering field strengths E_1 and E_2 are time-dependent functions $E_1(x, y; t)$, $E_2(x, y; t)$ of x and y.

By minimizing $P(t)$ of equation (1.7) with respect to the 'error signal'

$$\Delta\chi(t) = \chi(t) - \phi_0(t), \tag{1.10}$$

i.e. to the deviation of $\chi(t)$ from the main signal $\phi_0(t)$, one can derive, as an alternative form for (1.8),

$$\tan \Delta\chi(t) = \frac{\int\int E_1 E_2 \sin \tilde{\phi}\, dxdy}{\int\int E_1 E_2 \cos \tilde{\phi}\, dxdy}. \tag{1.11}$$

If we make the assumption that the two interfering beams have identical intensity profiles $I(x, y; t)$, i.e. the fields E_1 and E_2 differ only in their phase $\phi(x, y; t)$, then one can substitute $I(x, y; t)$ for the product $E_1 E_2$ in equations (1.8) and (1.11).

With the further assumption that the phase ripple $\tilde{\phi}(x, y)$ does not change drastically inside the spot illuminated by $I(x, y; t)$, we arrive at a linearized solution

$$\Delta\chi(t) = \frac{\int\int I(x, y; t)\tilde{\phi}(x, y)\, dxdy}{\int\int I(x, y; t)\, dxdy}, \tag{1.12}$$

the error signal $\Delta\chi(t)$ being represented by the original phase ripple $\tilde{\phi}(x, y)$ averaged over the photodiode surface with the locally fluctuating intensity $I(x, y; t)$ as weighting factor.

Finally, assuming that the intensity distribution $I(x, y; t)$ fluctuates by only a small amount $\delta I(x, y; t)$ around a constant time average $I_0(x, y)$, the fluctuation $\delta\chi(t)$ in the signal $\chi(t)$ becomes

$$\delta\chi(t) = \frac{\int\int \delta I(x, y; t)\tilde{\phi}(x, y)\, dxdy}{\int\int I_0(x, y)\, dxdy}. \tag{1.13}$$

2. Fluctuations of laser beam geometry

In this section, two types of fluctuations in the beam intensity distribution are considered, both of which lend themselves to simple geometrical interpretations. It is only after the discussion of these two special cases that a more general view is taken, as required for the understanding of the proposed mode selector scheme for reducing beam geometry noise.

2.1. *Lateral beam jitter*

Let us assume an incoming laser beam which, preserving its shape, moves laterally in the x-direction by a time-dependent distance $a(t)$: we have to substitute $I[x-a(t)]$ for $I(x)$. Furthermore, let us assume a tilt α_x between the two interfering wavefronts, then

$$\tilde{\phi}(x) = \alpha_x k x. \tag{2.1}$$

Such a tilt could, for instance, be the result of a misalignment of the beam splitter by an angle $\alpha_x/2$. Within the approximation of equation (1.13), the spurious signal due to the excursions $a(t)$ becomes

$$\delta\chi = \frac{\int \{I(x-a) - I(x)\}\alpha_x k x\, dx}{\int I(x)\, dx}, \tag{2.2}$$

which reduces, when the integration is taken from $-\infty$ to $+\infty$, to

$$\delta\chi(t) = \alpha_x k a(t). \tag{2.3}$$

This seemingly trivial result would, of course, also have followed from a model considering only a single ray, displaced sideways by $a(t)$, but here it has been derived for an arbitrary intensity profile $I(x)$.

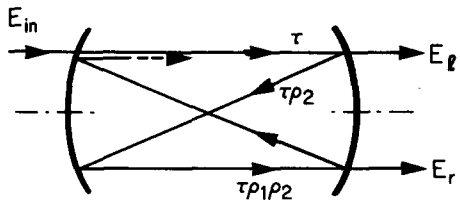

Figure 2. Confocal resonator used as beam symmetrizer.

The beam splitter can, in a rather straightforward procedure, be aligned such that the interfering wavefronts differ in tilt by less than $\alpha_x \simeq 10^{-5}$ rad. Adjusting and maintaining a tilt of 10^{-6} is about the best that can be done in our present set-up.

In the frequency range of interest (from a few hundred to a few thousand hertz), the laser beam exhibits lateral excursions $a(t)$ of the order of 10^{-9} m [2]. Although this is extremely small when compared with the width $2w$ of the laser beam ($2w \simeq 1{\cdot}5$ mm), the resulting noise $\delta\chi$ is thus one or two orders of magnitude above the eventual sensitivity goal of $\phi_g = 10^{-9}$ rad.

2.2. *The 'beam symmetrizer'*

The estimate of the noise contribution $\delta\chi(t)$ demonstrates clearly the need for reducing the lateral jitter $a(t)$ of the beam, before it enters the interferometer. A first step in that direction was the introduction of a 'beam symmetrizer' [5].

An optical resonator is placed into the light path, consisting of two confocal mirrors (figure 2), i.e. mirrors with a spacing d equalling their radius of curvature R. When tuned to the laser frequency, this resonator has a high transmittance for light components which are symmetrical with respect to its optical axis. A small lateral jitter $a(t)$ can be approximated by adding a small off-axis component $a(t)I'(x)$. In figure 2, the admixture of such an asymmetrical component is indicated schematically by a single incoming ray E_{in}. It splits up into two outgoing rays, symmetrical with respect to the optical axis, and with a ratio E_ℓ/E_r of their field strengths which is given by the product $\rho^2 = \rho_1\rho_2$ of the field reflectivities ρ_1 and ρ_2 of the two mirrors.

The relative field strength difference $(E_\ell - E_r)/(E_\ell + E_r)$, and thus the beam's lateral excursion, appears reduced by a factor

$$\frac{1}{S_1} = \frac{1-\rho^2}{1+\rho^2} \simeq \frac{1-\rho^2}{2\rho}. \tag{2.4}$$

With reflectances of $\rho^2 = 95$ per cent, the resulting suppression by a factor $S_1 \simeq 40$ was sufficient for our present requirements.

2.3. *Pulsation in beam width*

Another type of fluctuation in the intensity profile can be interpreted as a pulsation $\delta w/w$ in the beam width $2w$. For simplicity, let us consider a case where $I(x)$ is replaced by

$$(1+\kappa)I[(1+\kappa)x], \tag{2.5}$$

i.e. a case where only the width in the x-direction is affected, and, moreover, the total power is conserved.

In the frequency window from 500 Hz to a few kilohertz, our Ar^+ laser exhibited relative width variations $\delta w/w = \kappa(t)$ of the order of 10^{-6} [5].

The symmetrical beam pulsation (2.5) is an even function of x, and it leads to spurious signals $\delta\chi(t)$ only if the phase difference $\tilde{\phi}(x)$ between the wavefronts also includes even functions of x, in the simplest case

$$\tilde{\phi}(x) = cx^2. \tag{2.6}$$

An appropriate measure for the curvature of the phase ripple $\tilde{\phi}(x)$ is cw^2, for which an upper limit can be gained from a measurement of the light power at interference minimum. It was found to be of the order of 10^{-1} rad.

The spurious signal

$$\delta\chi = \frac{\int \{(1+\kappa)I[(1+\kappa)x] - I(x)\} cx^2\, dx}{\int I(x)dx} \tag{2.7}$$

becomes (neglecting a term in κ^2)

$$\delta\chi = -2\kappa c w^2 v^2, \tag{2.8}$$

where the numerical factor

$$v^2 = \frac{\int I(x)x^2\, dx}{w^2 \int I(x)\, dx} \tag{2.9}$$

depends on the model assumed for $I(x)$, but not very strongly. For an $I(x)$ constant from $-w$ to $+w$, one obtains $v^2 = 1/3$; for a gaussian, down to e^{-2} at $x = w$, v^2 would be 1/2; and for the slowly decreasing profile $I(x) = [1 + (x/w)^2]^{-2}$, we have $v^2 = 1$.

With the empirical data for $\kappa = \delta w/w$ and cw^2 as quoted above, equation (2.8) gives a noise contribution of about one power of 10 above the sensitivity goal of $\phi_g = 10^{-9}$. So the beam pulsation also calls for a suppression with similar effectiveness as we had been able to provide in the case of the lateral beam jitter.

The confocal optical resonator used there does not suppress the pulsations in beam width. We are particularly indebted to Dr. A. Brillet for pointing out that, by a different choice of mirror separation, the extreme degeneracy of the confocal case is lifted, and a strong suppression both of the lateral jitter and of the width pulsation is made possible.

The following sections will treat, in a more general way, the characteristics of spherical optical resonators, and how they can be used to suppress deviations from the ideal shape of a laser beam.

3. Modes in optical resonators

The view taken in this section can be summarized in the following manner. The laser beam, on its way to the interferometer, passes through a high-Q optical resonator. As viewed from this resonator, an incident field distribution $E(x, y; t)$ can be expanded into a series of eigenmodes $e_{mn}(x, y)$ with (possibly time-dependent) amplitudes $a_{mn}(t)$.

The desired fundamental mode $e_{00}(x, y)$ is a gaussian beam centred on the resonator's optical axis. By adjusting the mirror distance, the resonator will be tuned so that this fundamental mode has maximum transmission. The higher modes e_{mn}, describing the unwanted perturbations of the gaussian beam, will in general not be in resonance, and will thus be almost totally suppressed.

3.1. *Theory of optical resonators*

The theory of confocal optical resonators was first expounded simultaneously by Fox and Li [6] and by Boyd and Gordon [7], and later generalized by Boyd and Kogelnik [8].

Some formulae used below are taken from reviews and applications [9–11], but in general they are easily derived from the original representations.

3.2. *Notation*

The notation used by the authors quoted is not consistent, so we will start off by defining some of the symbols to be used below.

The optical resonator is composed of two highly reflective mirrors, separated by a distance d, and usually facing each other with their concave surfaces (figure 3 (a)). Their radii of curvature are denoted by R_1 and R_2 (or R if they are identical). As an important special case we have the confocal resonator, said to have the characteristic length b, if distance d and curvature radius R have a common value b (see figure 3 (b)).

The field propagates in the z-direction, i.e. in the optical axis interconnecting the centres of curvature of the two mirrors. The transverse directions are denoted by x and y, and the distance from the optical axis by $r=\sqrt{(x^2+y^2)}$. The lateral field distribution $E(x, y)$ of the beam will be expressed by normal modes which all have a common gaussian factor $\exp(-r^2/w^2)$. This factor is down to $1/e$ at the characteristic half-width w which is a function of z. Sometimes it is convenient to use the normalized transverse coordinates.

$$\xi=\frac{x}{w}, \quad \eta=\frac{y}{w}. \tag{3.1}$$

The mirror diameters are considered to be large compared with the beam widths.

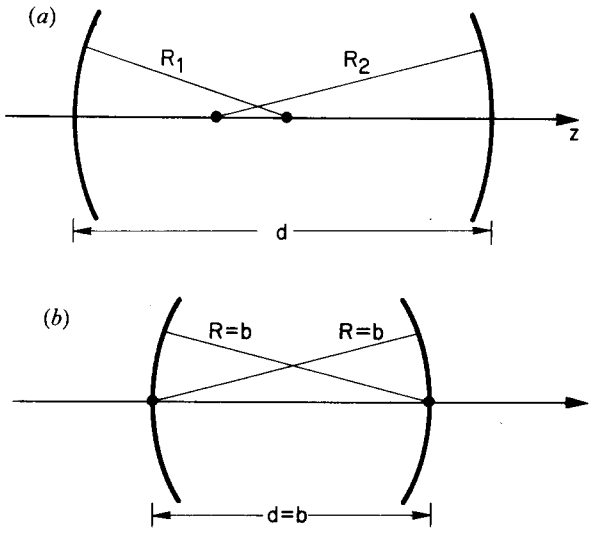

Figure 3. Optical resonators: (a) general configuration; and (b) confocal case.

3.3. *Modes in the confocal resonator*

Starting out from Huygens's principle, Boyd and Gordon [7] have determined self-consistent field patterns $E(x, y)$ such that a given field distribution on one mirror reproduces itself on the opposite mirror, allowing only a constant (possibly complex) factor. The problem can be formulated as an integral equation which, in the limit of infinite mirror diameters, is solved by normal modes $e_{mn}(x, y)$ that can be expressed as a product

$$e_{mn} \propto h_m(\xi) h_n(\eta) \tag{3.2}$$

of two gaussian–hermite functions of the type

$$h_m(\xi) = \frac{\Gamma(\frac{1}{2}m+1)}{\Gamma(m+1)} H_m(\sqrt{2}\xi) \exp(-\xi^2), \tag{3.3}$$

where the arbitrary factor $\Gamma(\frac{1}{2}m+1)/\Gamma(m+1)$ was chosen such that for even orders $m=2j$ we have $|h_{2j}(0)|=1$. The hermite polynomials H_m of the argument $\sqrt{2}\xi$ are defined by

$$H_m(\sqrt{2}\xi) = 2^{-m/2} \exp(2\xi^2) \left(\frac{-d}{d\xi}\right)^m \exp(-2\xi^2). \tag{3.4}$$

Figure 4 (*a*) shows the first three of the gaussian–hermite functions,

$$h_0(\xi) = \exp(-\xi^2); \quad h_1(\xi) = \sqrt{(2\pi)}\xi \exp(-\xi^2); \quad h_2(\xi) = (4\xi^2 - 1)\exp(-\xi^2),$$

and figure 4 (*b*), as examples of higher orders, $h_6(\xi)$ and $h_7(\xi)$.

When we add to the purely gaussian ground mode $h_0(\xi)$ a small contribution of $h_1(\xi)$ (of relative amplitude a_1) this is equivalent to a lateral shift of the beam axis by

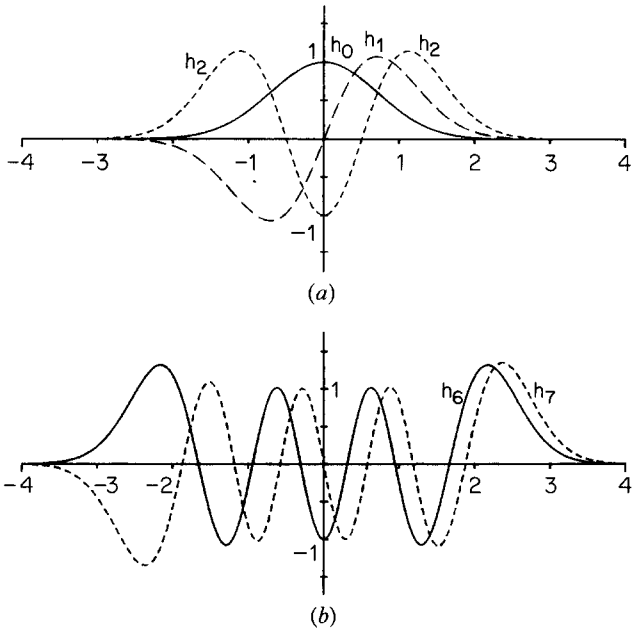

Figure 4. Gaussian–hermite functions: (*a*) $h_0(\xi)$, $h_1(\xi)$, $h_2(\xi)$; and (*b*) $h_6(\xi)$, $h_7(\xi)$.

$\delta\xi = \delta x/w\sqrt{(\pi/2)}a_1$. A small contribution of $h_2(\xi)$ (amplitude a_2), on the other hand, leads to a change in the beam width by $\delta w/w = 2a_2$. The phenomena of lateral beam jitter and pulsation in the beam width, discussed in the previous sections (§§2.1 and 2.3), are thus expressed as contaminations by low-order transverse modes.

3.4. *Non-confocal resonators*

From the field distributions (3.2) on the confocal mirrors, the field distribution at any value z can be calculated, again using Huygens' principle. With the use of the gaussian–hermite functions introduced above, Boyd and Gordon's equation (20) becomes very simple:

$$e_{mn}(x, y; z) = \frac{w_0}{w(z)} h_m\left(\frac{x}{w(z)}\right) h_n\left(\frac{y}{w(z)}\right) \times \exp\left(-i\left\{kz + (1+m+n)\psi(z) + \frac{kr^2}{2R(z)}\right\}\right), \tag{3.5}$$

with $w(z)$, $R(z)$ and $\psi(z)$ to be explained below.

If for the moment we ignore the phase factor, we see that the modes maintain their general appearance, only that all lateral dimensions of the field distribution are scaled by a common factor $w(z)$. At the waist of the beam, at $z=0$, the gaussian

$$\exp(-\xi^2 - \eta^2) = \exp(-r^2/w^2),$$

included in $h_m(\xi)h_n(\eta)$, has a $1/e$ radius w given by

$$w_0 = \sqrt{\frac{b}{k}} = \sqrt{\left(\frac{b\lambda}{2\pi}\right)}. \tag{3.6}$$

The minimum width w_0 is uniquely determined by the wavelength λ and the characteristic length b of the confocal resonator. As indicated in figure 5, the beam radius w increases with the distance z from the central plane according to

$$w(z) = w_0\sqrt{(1+\zeta^2)}. \tag{3.7}$$

Here, we have introduced the normalized longitudinal coordinate

$$\zeta = \frac{2z}{b} \tag{3.8}$$

to describe the propagation along the optical axis (z-axis), counting from the central plane.

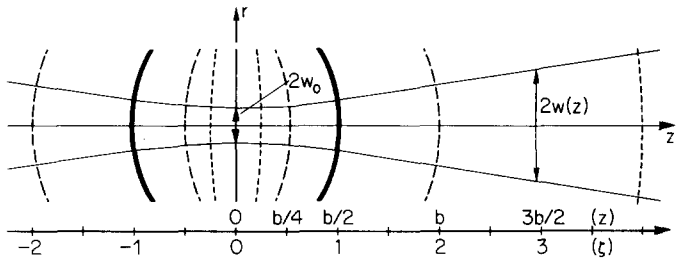

Figure 5. Gaussian beam and surfaces of constant phase.

The surfaces of constant phase have radii of curvature

$$R(z)=\frac{1+\zeta^2}{2\zeta}b=\left(\zeta+\frac{1}{\zeta}\right)\frac{b}{2}, \tag{3.9}$$

having a minimum ($R=b$) at the confocal distance $z=\pm b/2$ ($\zeta=\pm 1$), and approaching infinity (plane wave) at the beam waist ($z=0$), as well as at infinite distance ($z=\pm\infty$).

A gaussian beam with given propagation constant $k=2\pi/\lambda$ is fully determined for all values of z if at some distance z_0 from the beam's waist any two out of the (five) following variables are known:

$$b;\quad z_0;\quad \zeta_0=\frac{2z_0}{b};\quad R(z_0)=\left(\zeta_0+\frac{1}{\zeta_0}\right)\frac{b}{2};\quad w(z_0)=\sqrt{\left[\frac{b}{k}(1+\zeta_0^2)\right]}. \tag{3.10}$$

The mode pattern remains unchanged if one places two appropriately curved mirrors at any two of the surfaces of constant phase. The field distribution in the non-confocal resonator thus formed can be derived from an equivalent confocal resonator of characteristic length b, where b can be determined from R_1, R_2 and d with the relation

$$b^2=\frac{4d(R_1-d)(R_2-d)(R_1+R_2-d)}{(R_1+R_2-2d)^2}. \tag{3.11}$$

The condition that b^2 be positive describes the region of stable configurations, i.e. configurations in which the beam is being refocused on successive round trips, rather than becoming progressively more divergent.

3.5. *Mode selective Fabry–Pérot resonator*

The resonator can be treated as a Fabry–Pérot, in which the field, on each return trip $z_1\to z_2\to z_1$, is weakened by a factor $\rho_1\rho_2$, when ρ_1^2 and ρ_2^2 are the power reflectances of the two mirrors. We will from now on assume mirrors of equal reflectances, ρ^2, and of common transmittances τ^2.

In contrast to plane-wave optics, the light phase ϕ varies with z (or with ζ) not in a linear fashion $\phi(z)=kz$, but rather in the form

$$\phi(z)=kz+(1+m+n)\psi(z), \tag{3.12}$$

with

$$\psi(z)=\arctan\zeta. \tag{3.13}$$

The additional phase contribution $\Delta\phi=(1+m+n)\psi(z)$ has a high rate of change in a region around $z=0$, extending, say, out to $z=\pm b$.

What is important in our application is that $\Delta\phi$ depends on the mode order $N=m+n$, i.e. on the sum of the hermite indices m and n. This will allow us to discriminate between modes that have different orders N.

The resonator can be tuned, by fine adjustment of the mirror distance $d=z_1-z_2$, such that the ground mode ($N=0$) reproduces itself with zero phase difference

$$\Delta\phi_0=2kd+2(\psi_1-\psi_2)=0 \bmod 2\pi \tag{3.14}$$

on one return trip $z_1\to z_2\to z_1$.

For the higher modes $m+n>0$, the successive field contributions being superimposed are then out of phase by an angle

$$\Delta\phi_N=(m+n)2(\psi_1-\psi_2)=N2\Psi. \tag{3.15}$$

Here, Ψ stands for the single-trip phase difference

$$\Psi=\psi_1-\psi_2=\arctan\zeta_1-\arctan\zeta_2. \tag{3.16}$$

By adding up the field contributions one derives the fraction T_N of the incident power transmitted by this Fabry–Pérot resonator as

$$T_N=\frac{\tau^4}{(1-\rho^2)^2}\frac{1}{1+\left(\frac{2\rho}{1-\rho^2}\sin N\Psi\right)^2}, \tag{3.17}$$

which we will call the (power) 'throughput' to distinguish it from the single-mirror transmittance τ^2.

4. Choice of resonator parameters

In this section we will discuss some of the considerations in choosing the parameters of an optical resonator so that it best utilizes the mode selectivity expressed in equation (3.17).

4.1. *Mirror properties*

In equation (3.17), the first term $T_0=\tau^4/(1-\rho^2)^2$ is the power throughput at resonance. It would reach unity only for ideal mirrors in which power reflectance ρ^2 and power transmittance τ^2 add up to unity: $\rho^2+\tau^2=1$. In the presence of losses σ^2 (absorption or scattering), with $\rho^2+\sigma^2+\tau^2=1$, one can express T_0 by

$$T_0=\frac{1}{(1+\sigma^2/\tau^2)^2}. \tag{4.1}$$

For a high throughput T_0 of the ground mode, the losses σ^2 have to be small compared with the mirror transmittance τ^2, which in itself is a small quantity in our high-Q resonator. With a commercial resonator (Tropel, $\rho^2=95$ per cent), we were able to obtain a throughput T_0 of about 75 per cent, but better values are technically realizable.

The relative suppression of the non-fundamental modes ($N>0$) is determined by the second term in equation (3.17). We shall define it by the reverse square root of this second term:

$$S_N=\sqrt{\left[1+\left(\frac{2\rho}{1-\rho^2}\sin N\Psi\right)^2\right]}. \tag{4.2}$$

Unless the phase angle $N\Psi$ is extremely close to a resonance $N\Psi_0=0 \bmod \pi$, the suppression (in field amplitude) is

$$S_N\simeq\frac{2\rho}{1-\rho^2}\sin N\Psi=S_{\max}s_N.$$

With mirrors having a reflectance ρ^2 of 95 per cent, a maximum suppression of $S_{\max}=2\rho/(1-\rho^2)\simeq 40$ can be obtained, which is considered sufficient for our current needs (§ 2.2).

Should higher suppression ratios S_{max} be required, one can either increase the reflectance ρ^2 of the mirrors, or use two resonators in series. In both cases one will have to expect a deterioration in the throughput T_0 of the fundamental mode.

4.2. *The phase angle* Ψ

Perturbing modes of the orders $N=1$ and $N=2$ have a simple geometric interpretation, which allowed a direct measurement (cf. §§ 2.1 and 2.3). Even though their field strengths are about six powers of 10 below the fundamental mode, they nevertheless give rise to intolerable error signals. Thus, in the choice of an appropriate phase angle Ψ, one has to make sure that the modes with $N=1$ and $N=2$ are suppressed sufficiently, i.e. one wants $\sin\Psi$ and $\sin 2\Psi$ to be sufficiently far away from zero.

Modes of order higher than $N=2$ represent rather complicated patterns. It can be assumed that they are contained in the incoming beam with amplitudes that decrease rapidly with increasing N. Furthermore, in the interferometer they will become effective only in combination with a corresponding phase ripple of the interfering wavefronts.

The need to suppress modes of medium order ($N=3, 4$) has not yet been clearly established. But a suppression would be welcome, and it can be had at little extra expense by an appropriate choice of Ψ.

Using (3.16) and (3.8) and well-known addition theorems, one can express Ψ by

$$\cos\Psi=\sqrt{\left[\left(1-\frac{d}{R_1}\right)\left(1-\frac{d}{R_2}\right)\right]}. \tag{4.3}$$

The condition that the radicand be positive, and not exceed 1, leads to the same stability criteria as those derived from equation (3.11).

Figure 6 shows plots of $s_N=\sin N\Psi$ for $N=1,\ldots,4$ (for $N=5, 6$, only the zero crossings are indicated). From these curves (special cases of Lissajous' traces) one can pick values $\cos\Psi$ for which s_1 and s_2 have high values (above 0·5, say), and for which none of the further traces is very close to zero.

4.3. *Symmetrical resonator configurations*

In practical applications one prefers the symmetric configuration, i.e. resonators with mirrors of equal radii of curvature. For brevity, we will restrict the following discussion to this special case, in which (4.3) becomes

$$\cos\Psi=1-\frac{d}{R}=1-\delta. \tag{4.4}$$

Only $\delta=d/R$, the ratio between the mirror separation d and the radius of curvature, R, enters into Ψ.

In figure 6, the lower axis is denoted by this relative mirror separation $\delta=d/R=1-\cos\Psi$. Beneath it some representative resonator configurations are indicated.

The traces are symmetrical with respect to $\cos\Psi=0$, i.e. to the confocal case $d=R$. Here, the odd modes undergo maximum suppression $S_{max}=2\rho/(1-\rho^2)$, as all $|s_{2j+1}|=1$. The even modes, however, pass the Fabry–Pérot with no extra suppression, as all even-order traces s_{2j} vanish at $\cos\Psi=0$.

One has to go rather far in either direction, before the most important of the even modes, $N=2$, shows an appreciable suppression, e.g. to $|\cos\Psi|>0{\cdot}126$ for $|s_2|>0{\cdot}25$.

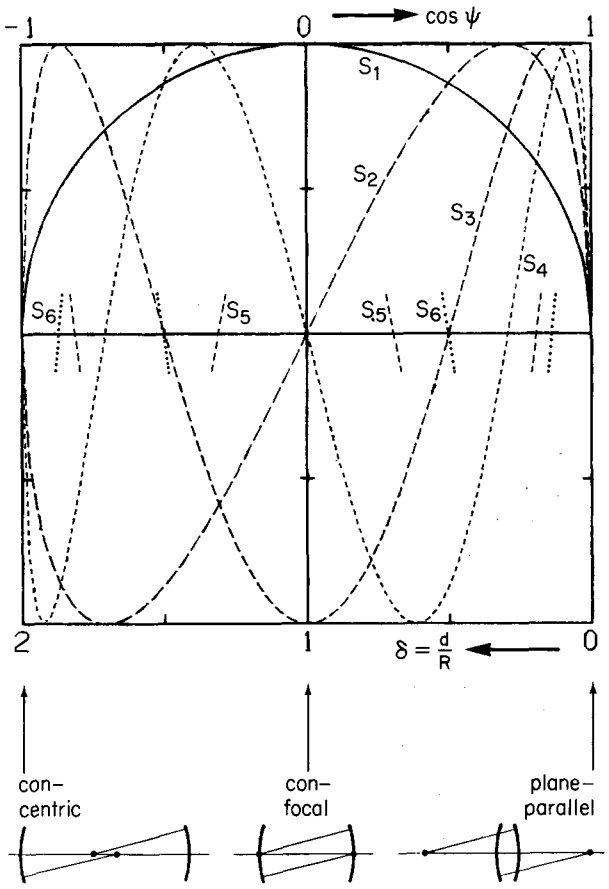

Figure 6. Coefficients $s_N = \sin N\Psi$, plotted versus $\cos\Psi$ (upper axis), or versus $\delta = 1 - \cos\Psi$ (lower axis). Three representative mirror configurations are indicated.

The plane-parallel limit ($\cos\Psi = 1$, $\delta = 0$) and the concentric limit ($\cos\Psi = -1$, $\delta = 2$) are degenerate with respect to all orders, so here we would have no mode selection at all. The suppression of the most important perturbing mode ($N = 1$) increases most slowly with departure from these limiting cases, but rapidly enough to assume values $s_1 > 0{\cdot}5$ in the range from $\cos\Psi = -0{\cdot}866$ to $\cos\Psi = +0{\cdot}866$ ($\delta = 0{\cdot}134$ to $\delta = 1{\cdot}866$).

Configurations that come close to the plane-parallel or concentric limits should be avoided anyway, for reasons of mechanical stability. Small tilts of the resonator mirrors would cause the optical axis to deviate strongly in its position (plane-parallel case) or in its direction (concentric).

Within the limits dictated by s_1 and s_2, one can easily pick configurations which provide reasonable suppression also for the medium-order modes.

4.4. *Mode matching*

In order to achieve a high throughput T_0, the beam emerging from the laser must be matched to the fundamental mode of the resonator. This matching can, for instance, be made with the help of a single adaptation lens as shown in figure 7.

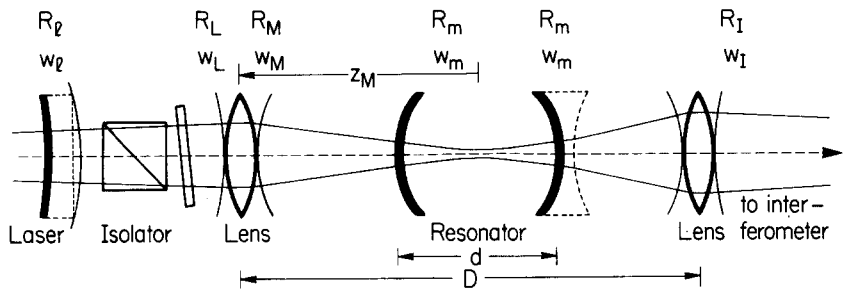

Figure 7. Matching of resonator modes (R_m, w_m) to given laser beam (R_ℓ, w_ℓ) and to requirements of the interferometer (R_I, w_I).

In calculations for this mode matching, repeated use must be made of the interrelations (3.10) between the characteristic variables of a gaussian beam.

From the configuration of the laser mirrors, one can derive the spot diameter $2w_\ell$ on the output mirror (with curvature radius R_ℓ). After passing through the mirror substrate and an optical isolator, the beam arrives with w_L and R_L at the adaptation lens.

In a similar fashion, one can trace the gaussian mode of the resonator (characterized by R_1, R_2, d) back to the position of the lens, and one must choose the distance z_M from waist to lens such that the mode radius w_M at the lens matches the actual beam radius w_L.

This choice of z_M also determines the radius of curvature, R_M. The matching in the curvature of the beams is provided by a lens with a focal length f given by

$$\frac{1}{f}=\frac{1}{R_L}+\frac{1}{R_M}. \tag{4.5}$$

In case of a mismatch, either in the curvature radii R of the phase fronts, or in the beam widths $2w$, the incoming field distribution $E(x, y)$, expanded with respect to the resonator modes, will have appreciable contributions in the non-fundamental modes ($N>0$). These extra modes are almost totally reflected, the loss in power throughput being proportional to the square of the relative mismatch $\delta R/R$ or $\delta w/w$ respectively. This loss becomes negligible when the relative mismatch is below, say, 10 per cent.

4.5. *Power density on optical surfaces*

In our application, we want to transmit high laser powers P, at present about 1 W, and perhaps up to 100 W in the eventual experiment. Intensities (power densities) $I=P/\pi w^2$ above an I_{max} in the order of 10 W/mm^2 can inflict thermal damage on the multi-layer coatings. So we have to keep the spot area πw^2 on the mirrors above

$$\pi w_m^2=\frac{P}{I_{max}}. \tag{4.6}$$

For mirrors of a given curvature radius R, the equations (3.7) and (3.6) define a characteristic spot radius

$$W_R=\sqrt{\left(\frac{2R}{k}\right)}=\sqrt{\left(\frac{R\lambda}{\pi}\right)}, \tag{4.7}$$

describing the spot size on the mirrors in a confocal arrangement ($d=R, \zeta=1$).

The intensity in such a confocal arrangement would be

$$I_R = \frac{P}{R\lambda}. \tag{4.8}$$

For the same mirrors in a non-confocal configuration ($d \neq R$), one can derive from (3.7) and (3.9) that the ratio of actual spot area πw^2 to the 'confocal' spot area πW_R^2 is

$$\frac{w^2}{W_R^2} = \zeta = \frac{d}{b}. \tag{4.9}$$

Thus, only configurations with sufficiently high

$$\zeta > \zeta_{\min} = \frac{P}{R\lambda I_{\max}} \tag{4.10}$$

are allowed, i.e. configurations with relative mirror separations

$$\delta_{\min} = \frac{d_{\min}}{R} > \frac{2\zeta_{\min}^2}{1+\zeta_{\min}^2}. \tag{4.11}$$

In an example with $P = 1\,\mathrm{W}$, $I_{\max} = 5\,\mathrm{W/mm^2}$, $R = 0{\cdot}1\,\mathrm{m}$, $\lambda = 0{\cdot}514 \times 10^{-6}\,\mathrm{m}$, we have $\zeta_{\min} = 3{\cdot}9$. The resulting configuration has a relative mirror separation of $d_{\min}/R = 1{\cdot}88$, which is about as close to the concentric limiting case as one would dare to go, from the considerations of mode suppression and mechanical stability discussed in § 4.3. With mirrors of curvature radius less than $R_{\min} = 0{\cdot}1\,\mathrm{m}$, one would no longer be able to reconcile these requirements.

4.6. *Structural length*

A further consideration in the implementation of a mode selector is the length d of the resonator and the overall length D required for mode matching.

If, from considerations of mode suppression and power density, minimum values for $s_1 = \sin\Psi$ and spot diameter $2w_m$ are given, the mirror spacing $d_{\min}$ of a (symmetrical) resonator becomes

$$d_{\min} = \frac{kw_m^2}{2} s_1. \tag{4.12}$$

With $w_m = 0{\cdot}25\,\mathrm{mm}$ and $s_1 = 0{\cdot}5$, we arrive at a resonator of length $d = 0{\cdot}19\,\mathrm{m}$, to be realized with mirrors of a curvature radius of either $R_c = 0{\cdot}10\,\mathrm{m}$ (near concentric case), or $R_p = 1{\cdot}43\,\mathrm{m}$ (near plane-parallel).

For an estimate of the overall length D, including the mode-matching optics, we have to make a few further assumptions. In our application, the beam coming from the laser has similar characteristics (R_L, w_L) as those required for the Michelson interferometer (R_I, w_I). In a completely symmetric configuration, the overall length D equals $2z_M$ (see figure 7).

If only one mode matching lens each (at $z = \pm z_M$) is used, the overall length can be approximated by

$$D \simeq \frac{kw_m w_L}{2} s_1. \tag{4.13}$$

With $w_m = 0{\cdot}25\,\mathrm{mm}$, $w_L = 0{\cdot}75\,\mathrm{mm}$ and $s_1 = 0{\cdot}5$, the total length D would be $0{\cdot}57\,\mathrm{m}$. This length can be reduced by the use of a diverging lens near the resonator mirrors.

By using plane-concave or symmetric bi-concave substrates for the resonator mirrors (the latter case being indicated in figure 7 for the right-hand resonator mirror) one can reduce D to 0·48 and 0·40 m respectively.

In our current gravitational wave experiment, bi-concave mirror substrates are going to be used, both radii of curvature being 0·10 m. The adaptation lenses will then need focal lengths of 0·15 m.

4.7. *Performance*

The suppression of the low-order modes was tested with a commercial optical resonator (Tropel, $R=50$ mm), at reduced laser powers to avoid damage to the optical coatings. The transmittance τ^2 of the mirrors is approximately 6 per cent, and to explain the resonance throughput of only 50 per cent we have to assume losses σ^2 of 2·5 per cent. This surprisingly high value may be due to an inadvertent thermal damage. With the resulting reflectance of $\rho^2=91{\cdot}5$ per cent we find a maximum suppression $S_{\max}=2\rho/(1-\rho^2)$ of 22·5.

The resonator was operated at its maximum mirror spacing of $d=61$ mm, a configuration rather close to the confocal case, with a first-order coefficient $s_1=0{\cdot}975$, and reasonable coefficients s_N for the next few orders N.

As pointed out in § 3.3, an admixture of a first-order mode (of relative field amplitude a_1) results in a lateral beam jitter (by $\delta x/w=1{\cdot}25a_1$). This jitter can be measured with a position-sensitive photodiode. Two plots of the spectral distribution of this jitter are shown in figure 8, with and without the mode selector. The spikes near 1·8 kHz represent an artificially introduced lateral jitter which clearly confirms the expected suppression by $s_1S_{\max}=22$. The continuous spectrum with mode selector (lower trace) is dominated by additional perturbations such as shot noise and harmonics of the 50 Hz mains, making a judgement of the suppression impossible. For the modes of order $N=2$ (the width pulsation), and even more so for the higher modes, measurement as well as artificial generation become much more difficult. The suppression of such higher modes has been checked only qualitatively, by observing that despite gross variations in the incoming beam shape (shadowing by masks) the outgoing beam maintained a sufficiently gaussian appearance of practically constant width.

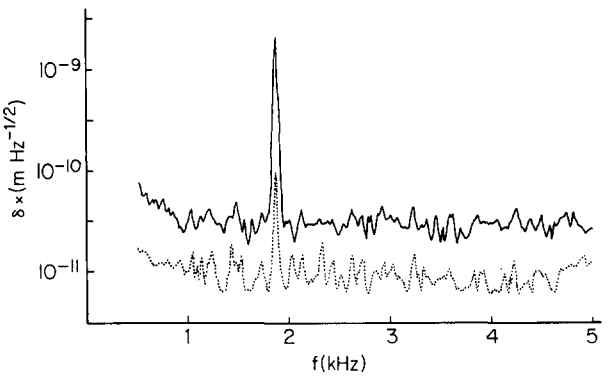

Figure 8. Spectrum of lateral beam jitter, without (upper trace) and with (lower trace) mode selection.

Notre développement d'un détecteur d'onde gravitationnelle nécessite un interféromètre de Michelson d'extrême sensibilité capable de mesurer 10^{-6} m (c'est-à-dire quelques 10^{-10} de la longueur d'onde de la lumière d'éclairage). Même après des réglages délicats des pièces composant l'interféromètre, et après de considérables améliorations de la stabilité du laser, des bruits très supérieurs au but à atteindre ont été observés, qui provenaient des fluctuations de la géométrie du faisceau laser. Les deux principaux types de fluctuations géométriques du faisceau sont une oscillation latérale et une pulsation en largeur du faisceau; ceci conduit à des signaux d'interféromètre perturbés si les fronts d'onde qui interfèrent sont mal réglés en direction et en courbure respectivement.

La géométrie du faisceau peut être considérablement stabilisée en le faisant passer au travers d'un résonateur optique. Les fluctuations géométriques du faisceau, vues de ce résonateur, peuvent être considérées comme un mode fondamental bien centré TEM_{00}, altéré par des modes transverses TEM_{mn}, dont les amplitudes décroissent rapidement avec les ordres m et n. Le résonateur, dans le cas le plus simple, consiste en deux miroirs concaves identiques de facteur de réflexion élevé ρ^2. La distance des miroirs peut être choisie de manière que, lorsque le résonateur est accordé pour que la transmission soit maximale pour le mode TEM_{00}, les modes transverses TEM_{mn} d'ordres inférieur soient presque totalement supprimés leurs amplitudes étant réduites par un facteur de l'ordre de $1-\rho^2$. Des considérations conduisant à une mise en oeuvre pratique sont discutées et des résultats expérimentaux sont donnés.

Unsere Entwicklung eines Gravitationswellen-Detektors erfordert ein Michelson-Interferometer mit einer Empfindlichkeit bis herab zu 10^{-16} m, also etwa 10^{-10} einer Wellenlänge λ des beleuchtenden Laserlichts. Selbst nach sorgfältiger Ausrichtung der Interferometer-Komponenten, und nach erheblichen Verbesserungen in der Laserstabilität, wurden noch Störsignale beobachtet, die weit über dieser angestrebten Empfindlichkeit lagen. Diese Störsignale rühren u.a. von Schwankungen der Laserstrahl-Geometrie. Zwei typische Beispiele für solche Schwankungen sind (*a*) ein seitliches Wackeln der Strahl-Position, und (*b*) ein Pulsieren des Strahl-Durchmessers; sie führen zu Störsignalen im Interferometer, wenn die interferierenden Wellenfronten fehlangepaßt sind bezüglich ihrer Richtung (*a*), bzw. bezüglich ihrer Krümmung (*b*).

Die geometrische Stabilität kann wesentlich verbessert werden, wenn man den Laserstrahl einen optischen Resonator durchlaufen läßt. Aus der Sicht dieses Resonators können die Geometrie-Schwankungen beschrieben werden durch einen wohlzentrierten Grund-Modus TEM_{00}, verunreinigt durch höhere Moden TEM_{mn}, mit Amplituden, die rasch mit zunehmender Ordnung $m+n$ abfallen. Der Resonator besteht im einfachsten Fall aus zwei identischen Hohlspiegeln hoher Reflektivität ρ^2. Der Spiegelabstand läßt sich so wählen, daß—bei Abstimmung auf maximale Transmission für den Grund-Modus TEM_{00}—die Transversal-Moden TEM_{mn} niedriger Ordnung $m+n$ fast vollständig unterdrückt werden, nämlich um Amplituden-Faktoren der Größenordnung $1-\rho^2$. Gesichtspunkte, die bei einer praktischen Ausführung zu beachten sind, werden diskutiert, und experimentelle Ergebnisse werden wiedergegeben.

References

[1] Winkler, W., 1977, *Proceedings of the International Symposium on Experimental Gravitation*, Pavia (Rome: Accademia Nazionale dei Lincei), pp. 351–363.
[2] Billing, H., Maischberger, K., Rüdiger, A., Schilling, R., Schnupp, L., and Winkler, W., 1979, *J. Phys.* E, **12,** 1043.
[3] Moss, G. E., Miller, L. R., and Forward, R. L., 1971, *Appl. Optics*, **10,** 2495.
[4] Weiss, R., 1972, *Q. Prog. Rep. Res. Lab. Electron., M.I.T.*, **105,** 54.
[5] Maischberger, K., Rüdiger, A., Schilling, R., Schnupp, L., Winkler, W., and Billing, H., 1980, *Proceedings of the Second Marcel Grossmann Meeting*, Trieste, edited by R. Ruffini (in the press); preprint MPI-PAE/Astro 209.
[6] Fox, A. G., and Li, T., 1961, *Bell Syst. tech. J.*, **40**, 453.
[7] Boyd, G. D., and Gordon, J. P., 1961, *Bell Syst. tech. J.*, **40**, 489.
[8] Boyd, G. D., and Kogelnik, H., 1962, *Bell Syst. tech. J.*, **41,** 1347.

[9] Röss, D., 1969, *Lasers, Light Amplifiers and Oscillators* (London, New York: Acad Press).
[10] Abderrazik, J.-E., 1967, *Annls Télécommun.*, **22,** 41.
[11] Fork, R. L., Herriot, D. R., and Kogelnik, H., 1964, *Appl. Optics*, **3,** 1471.